All-Optical Nanomechanical Heat Engine

Andreas Dechant,[1] Nikolai Kiesel,[2] and Eric Lutz[1]
[1]Department of Physics, Friedrich-Alexander-Universität Erlangen-Nürnberg, D-91058 Erlangen, Germany
[2]Vienna Center for Quantum Science and Technology (VCQ), Faculty of Physics, University of Vienna, A-1090 Vienna, Austria
(Received 17 September 2014; published 6 May 2015)

We propose and theoretically investigate a nanomechanical heat engine. We show how a levitated nanoparticle in an optical trap inside a cavity can be used to realize a Stirling cycle in the underdamped regime. The all-optical approach enables fast and flexible control of all thermodynamical parameters and the efficient optimization of the performance of the engine. We develop a systematic optimization procedure to determine optimal driving protocols. Further, we perform numerical simulations with realistic parameters and evaluate the maximum power and the corresponding efficiency.

DOI: 10.1103/PhysRevLett.114.183602 PACS numbers: 42.50.Wk, 05.40.Jc, 05.70.Ln, 37.10.Pq

During the last decade, significant progress in the fabrication of mechanical devices at the micro- and nanoscale has been achieved [1]. While this development enabled a plethora of technological applications, it also allows new experiments at the foundations of modern physics. These devices operate in a regime where thermal fluctuations are relevant, a situation which requires appropriate theoretical tools. In this direction, research in stochastic thermodynamics has been very successful at extending the laws of macroscopic thermodynamics to the level of single trajectories [2,3]. The discovery of fluctuation theorems has further opened the way to a systematic investigation of far-from-equilibrium processes [4,5]. On the other hand, experiments with nano- and micromechanical objects have entered the domain where quantum fluctuations dominate. Important examples are the recent achievements of the cooling of mechanical oscillators to the ground state [6–8] and the experimental demonstration of quantum state preparation [6] and entanglement generation [9].

A paradigmatic system for the study of stochastic thermodynamics is optically trapped micro-and nanobeads [3–5,10]. Optical tweezers enable fast control of the potential landscape experienced by the particles and accurate recording of their trajectories. In a pioneering experiment, this approach has been used to demonstrate a classical micromechanical Stirling engine [11], where the temperature of the liquid heat bath was controlled by laser absorption. While this is a very natural environment, there are limitations on the accessible parameter regime for the temperature and the optimization of the protocols used to implement the thermodynamic cycle.

The future realization of quantum heat engines requires the investigation of much more isolated systems. Towards this end, a concrete experiment of building an Otto heat engine using a single ion in a Paul trap has been put forward [12,13]. This ion is completely isolated from its natural environment, which is substituted by a reservoir of light that is engineered via Doppler cooling. More recently, a scheme to realize an optomechanical quantum heat engine that operates on polariton modes in the strong coupling regime has been suggested [14].

In this Letter, we propose a levitation approach to nanomechanical heat engines. Submicron particles are optically trapped in a moderate vacuum in a harmonic potential with a variable frequency. The heat bath is provided by a thermal environment (the rest gas inside the trap) in combination with optomechanical cavity cooling [15–20], which provides additional tunable damping. The motion of the particle is underdamped (in contrast to the experiment in Ref. [11]) and is only weakly coupled to the optical cavity, reducing dissipative effects. Altogether, this approach combines the excellent control offered by optical trapping with the fast optomechanical control of the center-of-mass temperature provided by cavity cooling. This allows flexibility in optimizing the heat engine and gives access to a large temperature regime, in principle, down to the quantum ground state. Optimization is an essential tool for maximizing the performance of a machine given existing constraints [21]. In the overdamped regime, the thermodynamic optimization problem has been solved for harmonic [22] and nonharmonic [23] systems. Explicit optimal protocols have been obtained for the Carnot cycle [24] but, to our knowledge, have never been implemented experimentally. By contrast, optimization in the underdamped case is notoriously more difficult [25], owing to the larger parameter space, and has been little explored. In the following, we begin by describing the working principles of an all-optical optomechanical heat engine. We present a systematic procedure for determining the driving protocol that maximizes the power output and evaluating the corresponding efficiency at maximum power. Finally, we numerically simulate the operation of the engine for a state-of-the-art levitated optomechanical system [26] and discuss the occurrence of jumps in the optimal protocols.

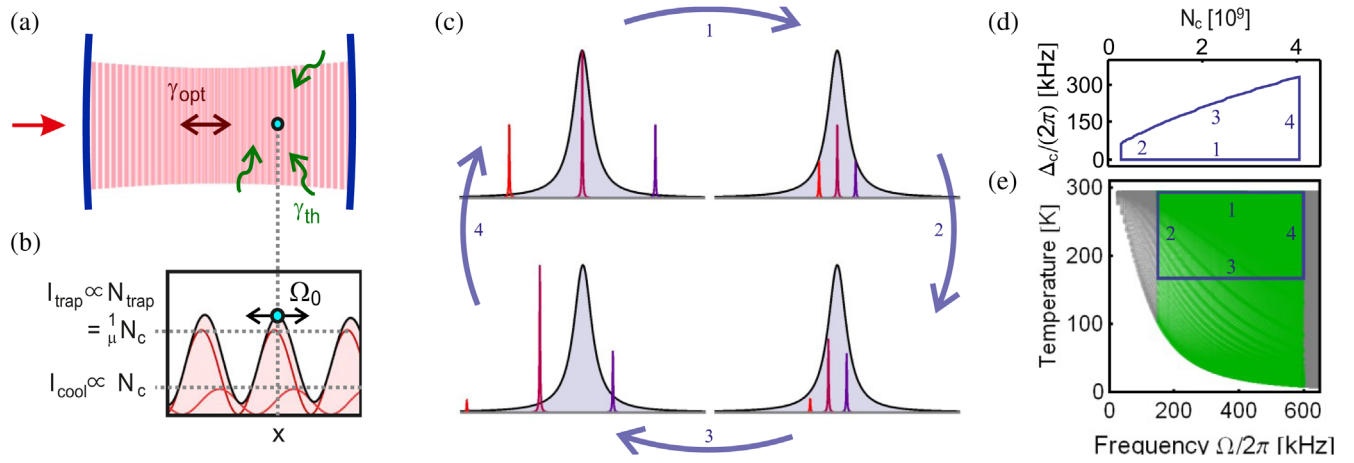

FIG. 1 (color online). Implementation of a Stirling cycle by cavity cooling of a levitated particle. (a) The nanoparticle is levitated in the optical field inside a Fabry-Perot cavity driven by two lasers that address subsequent longitudinal modes (cooling and trapping beam). Collisions with air molecules couple the center-of-mass motion of the particle to the thermal environment at room temperature with a damping rate γ_{th}. Additional damping γ_{opt} is provided by optomechanical coupling. (b) The combined intensity distribution of the two fields defines the optical trap position and frequency Ω_0. Optomechanical coupling to the cooling mode is ensured by a phase shift between the two modes at the particle position. (c) Cooling is achieved by an enhanced scattering of photons into the blue sideband when the cooling beam is red detuned from cavity resonance. (d) The cycle in terms of the control parameters (N_c, Δ_c). (e) The resulting Stirling engine cycle consists of two isothermal and two isochoric processes. We restrict the accessible frequencies for the optimization procedure to values that can be directly achieved in a recent experiment [26] (green shaded area, see Table I); however, a wider range of parameters should be easily accessible.

Optomechanical heat engine.—We consider a nanoparticle trapped in the optical cavity shown in Fig. 1(a). In our scenario, the particle is well confined inside the optical trap such that its center-of-mass motion $x(t)$ can be described by a harmonic oscillator of frequency Ω_0 in a thermal environment. Optomechanical interaction between the light field in the cavity and the mechanical oscillator modifies its spring constant and damping [27,28]. We describe the system by the following effective Langevin dynamics with the additional damping term due to sideband cooling

$$\ddot{x} + (\gamma_{\mathrm{th}} + \gamma_{\mathrm{opt}})\dot{x} + \Omega^2 x = F_{\mathrm{th}}/m. \tag{1}$$

Here, γ_{th} (γ_{opt}) denotes the damping coefficient due to the surrounding gas (sideband cooling), Ω the effective frequency of the oscillator, m the mass of the nanoparticle, and F_{th} a white noise force generated by the collisions with the surrounding gas at temperature T [29]. Typical experimental parameters are summarized in Table I. The steady temperature of the particle is given by $T_{\mathrm{eff}} = T\gamma_{\mathrm{th}}/\gamma_{\mathrm{eff}} < T$.

The proposed experimental scheme for the realization of the engine is sketched in Figs. 1(a) and 1(b). A submicron particle is optically trapped at the intensity maximum of two standing waves in the cavity field whose intensity maxima are shifted in position with respect to each other. One of the fields (cooling field) serves for cavity cooling and can be driven detuned from the cavity resonance for that purpose. The other field (trapping field) is always driven with a resonant beam and does not directly participate in the optomechanical interaction. The cooling beam is used to control the optomechanical damping γ_{opt} by its power P_c and detuning Δ_c. This particular case of a self-trapping approach has recently been demonstrated experimentally in Ref. [26]. The optomechanical coupling between cooling field and nanoparticle can not only be used to manipulate, but also to detect its motion. The axial motion of the particle generates a phase modulation of the cooling beam, which can be detected by heterodyne detection in transmission of the cavity [26]. In this way, it is possible to obtain the time-resolved trajectory of the particle and, thus, evaluate all the thermodynamic quantities, like heat, work, efficiency, and power of the engine with the help of stochastic thermodynamics [2,3].

The frequency Ω_0 of the mechanical resonator is determined by the occupation N_c and N_t of the cooling and trapping modes, respectively. In addition, the optical spring effect results in a shift of the mechanical frequency

TABLE I. Values of the control parameters $(\Omega, T_{\mathrm{eff}})$ of the heat engine and (N_c, Δ_c) of the optomechanical systems used in the numerical simulations. The parameters for the cycle are the values just after the indicated steps. Further experimental parameters are $T = 293$ K, $\gamma_{\mathrm{th}}/2\pi = 1.80$ kHz (at $\sim$1 mbar), $\gamma_{\mathrm{opt}}/2\pi = 1.35$ kHz, and the cavity linewidth $\kappa/2\pi = 180$ kHz.

Cycle step	T_{eff} (K)	$\Omega/2\pi$ (kHz)	$\Delta_c/2\pi$ (kHz)	$N_c/10^8$
$4 \to 1$	293	600	0	40.6
$1 \to 2$	293	150	0	2.54
$2 \to 3$	167	150	64.3	2.53
$3 \to 4$	167	600	334	40.4

$\Omega_0 \to \Omega$ and depends on the detuning Δ_c [16,31]. For simplicity, we keep the position of the optical trap fixed, which can be achieved by keeping the ratio of the photon occupation of the cooling and trapping mode constant at $\mu = N_c/N_t$ [see Fig. 1(b) and [32]].

The temperature of the particle may be regulated via sideband cooling. For the above experimental configuration, the theory of sideband cooling for standard clamped optomechanics [15–20,26] directly applies. In this scheme, the oscillating particle scatters photons into optical sidebands of frequencies $\omega_c \pm \Omega$ at rates $A_\pm$, known as Stokes and anti-Stokes scattering, respectively. For $\Delta_c > 0$ (red detuning), anti-Stokes scattering dominates Stokes scattering. This process results in a damping of the center-of-mass motion of the particle with an additional friction coefficient $\gamma_{opt} = A_- - A_+$ that can be easily varied via the cavity detuning Δ_c.

The two thermodynamic parameters of the optomechanical heat engine, the frequency Ω, and the optical damping γ_{opt} (which sets the effective temperature T_{eff}), can, thus, be directly tuned via the two control parameters of the experiment, the detuning Δ_c and the power of the cooling laser, which governs N_c. A Stirling cycle that consists of two isochoric and two isothermal transformations may then be implemented through the following steps: (1) The particle interacts with a bath at constant temperature T via the coupling γ_{th} (both laser fields are resonant, $\Delta_c = 0$). The frequency Ω is lowered during time τ_{hot} by changing the cavity fields from the high initial value $N_{c,h}$ to the lower value $N_{c,l}$. (2) The temperature of the bath is reduced to T_{eff} by detuning the cooling laser to $\Delta_{c,l}$. The frequency Ω is kept constant. (3) The particle interacts with a bath at constant temperature T_{eff} via the coupling γ_{eff}. The frequency Ω is increased to its initial value during time τ_{cold} by enhancing the cavity fields from $N_{c,l}$ to N_{c,h_Δ}. The detuning Δ_c is adjusted to keep γ_{opt} constant [Fig. 1(d)]. (4) In the last isochoric step, all control parameters are switched back to their initial values.

The above cooling-heating sequence based on sideband cooling is illustrated in Fig. 1(c). The Stirling cycle is shown in Fig. 1(e) for the thermodynamic parameters (Ω, T_{eff}), and in Fig. 1(d) for the control parameters (N_c, Δ_c). A summary of the values used in the simulations (see Figs. 2 and 3) is given in Table I. (See [32] for details on the equations and experimental aspects).

Optimal protocols.—Next, we shall determine the driving protocol that maximizes the power output of the engine. We begin by writing the mean heat exchanged between the particle and bath during a time interval $[t, t+\tau]$ [2,3]

$$Q = \gamma_{th} k_B T \tau - m\gamma_{eff} \int_t^{t+\tau} dt' \sigma_v(t'), \qquad (2)$$

where $\sigma_v(t) = \langle v^2(t) \rangle$ is the mean-square velocity of the particle. The work done by the engine during a full cycle is $-W = Q_{hot} + Q_{cold}$. The power and efficiency are accordingly

$$\mathcal{P} = \frac{Q_{hot} + Q_{cold}}{\tau_{hot} + \tau_{cold}}, \qquad \eta = 1 + \frac{Q_{cold}}{Q_{hot}}. \qquad (3)$$

In order to compute the above quantities, we need to evaluate the dynamics of $\sigma_v(t)$ in Eq. (2). Multiplying the Langevin equation (1) by v, respectively, x, and taking the ensemble average, we obtain the two equations

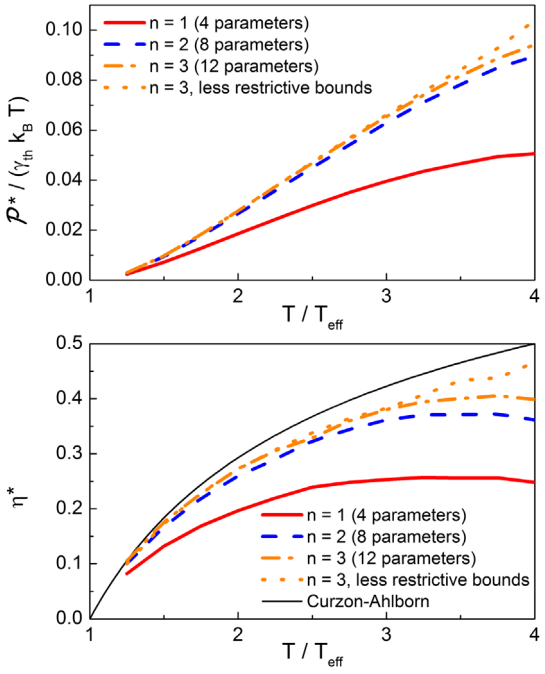

FIG. 2 (color online). Power $\mathcal{P}^*$ and efficiency at maximum power η^* as a function of the ratio of the bath temperatures, T/T_{eff}, for various optimization steps, $n = 1, 2$, and 3. The dotted line shows the performance for $n = 3$ without the experimental constraints on the rate of frequency change.

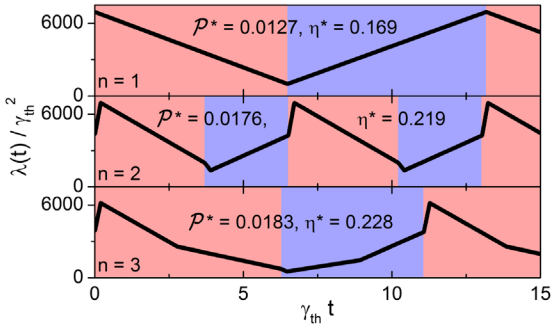

FIG. 3 (color online). Optimal driving protocols $\lambda(t)$ for a temperature ratio $T/T_{eff} = 1.75$ and the same parameters as in Fig. 2 (top to bottom). The red (blue) shaded regions denote coupling to the hot (cold) bath, the corresponding power output $\mathcal{P}^*$ (in units of $\gamma_{th}T$) and efficiency η^* are also stated. Fast frequency variations occur at the transitions between hot and cold baths for higher-order optimization.

$$\dot{\sigma}_v + 2\gamma_{\rm eff}\sigma_v + 2\lambda\dot{\sigma}_x = \frac{2\gamma_{\rm eff}k_B T_{\rm eff}}{m}, \tag{4a}$$

$$\ddot{\sigma}_x + \gamma_{\rm eff}\dot{\sigma}_x + \lambda\sigma_x - 2\sigma_v = 0, \tag{4b}$$

where $\sigma_x = \langle x^2(t)\rangle$ is the mean-square displacement and $\lambda(t) = \Omega^2(t)$ the spring constant of the oscillator. We choose the latter as the control parameter for maximizing the power $\mathcal{P}$. The steady state solutions of Eqs. (4) are given by $\sigma_v = \lambda\sigma_x = k_B T_{\rm eff}/m$ corresponding to equilibrium at temperature $T_{\rm eff}$. In the overdamped limit, $\gamma_{\rm eff} \gg \Omega$, the velocity thermalizes quasi-instantaneously and the dynamics can be described in terms of the slow position variable only. In this regime, the optimal protocol $\lambda(t)$ can be obtained analytically [24]. By contrast, in the underdamped limit, $\gamma_{\rm eff} \ll \Omega$, the search for the optimal protocol requires solving a set of coupled, nonlinear differential equations for $\lambda(t)$ with periodic boundary conditions, a task which is daunting, even numerically.

We tackle this challenge by introducing piecewise linear trial protocols $\lambda(t)$ with $n = 1, 2, 3, \ldots$. linear segments that we optimize numerically. This systematic expansion allows us to find the optimal protocol to any desired accuracy. The limit $n \to \infty$ corresponds to the true optimal protocol. As we will show, the expansion converges rapidly to a stable solution (see Fig. 2). The first term, $n = 1$, is a linear change of $\lambda(t)$ during the coupling to both hot and cold baths

$$\lambda(t) = \begin{cases} \frac{(\lambda_2-\lambda_1)t}{\tau_{\rm hot}} + \lambda_1, & 0 < t < \tau_{\rm hot} \\ \frac{(\lambda_1-\lambda_2)(t-\tau_{\rm hot})}{\tau_{\rm cold}} + \lambda_2, & 0 < t - \tau_{\rm hot} < \tau_{\rm cold}. \end{cases} \tag{5}$$

This simple linear protocol depends on the four parameters $\tau_{\rm hot}$, $\tau_{\rm cold}$, λ_1, and λ_2. We find the maximum power $\mathcal{P}^*$ and the corresponding efficiency η^* by numerically solving Eqs. (4) for this protocol, computing the corresponding power output and optimizing with respect to the four parameters, keeping the ratio of the temperatures of the two baths, $T/T_{\rm eff}$, fixed, see [32]. For the second term, $n = 2$, we subdivide each of the two linear pieces of the protocol into two parts, giving a total of eight parameters to optimize. We may continue this systematic procedure by subdividing each linear segment into n parts. Figure 2 shows the maximum power $\mathcal{P}^*$ and the corresponding efficiency η^* as a function of the temperature ratio $T/T_{\rm eff}$, for $n = 1, 2$, and 3. We have performed the numerical optimization by taking the experimentally accessible range of parameters displayed in Fig. 1(e) into account. We observe that both power and efficiency at maximum power are significantly improved when going from $n = 1$ (four parameters) to $n = 2$ (eight parameters). However, the performance of the engine is only slightly enhanced by adding an additional term (12 parameters), indicating that the expansion converges quickly [37]. Interestingly, the efficiency at maximum power is bounded by the Curzon-Ahlborn efficiency, $\eta_{\rm ca} = 1 - \sqrt{T_{\rm eff}/T}$ [38], which it approaches for small temperature differences.

The optimal protocols found for $n = 1, 2$, and 3 are shown in Fig. 3 for the parameters given in Table I. We note, again, a substantial difference between $n = 1$ and $n = 2$, and minor changes when going to higher orders. The coupling times to hot and cold baths are generally not equal, since $\gamma_{\rm eff} > \gamma_{\rm th}$. The most striking difference is the appearance of fast variations of the frequency at the transitions between hot and cold baths. Discontinuities in the optimal driving protocol were predicted in the overdamped regime [24]. These jumps are interesting, since they are absent in a linear response approach, and their occurrence is, therefore, a hallmark of far-from-equilibrium behavior [3]. From a physical point of view, fast frequency variations permit an almost instantaneous change of the mean-square velocity of the particle, and, hence, reduce dissipation and increase engine performance [25]. We note that the frequency jumps occur due to the instantaneous changes in temperature during the isochoric steps, which maximize the power output. In the experimental system, both the frequency jumps and the instantaneous temperature switching can only be realized in an approximate manner. If the relative rate of change in the frequency, $\dot{\Omega}/\Omega$, becomes larger than the cavity decay rate, transients in the cavity field have to be taken into account. This experimental restriction limits the attainable power and efficiency at large temperature differences compared to the unrestricted system (dotted line in Fig. 2). Nevertheless, the essential role of the frequency jumps in enhancing the performance of the heat engine should be testable in the experiment by evaluating efficiency and power for different driving protocols (with and without jumps).

Conclusions.—We have introduced a concrete experimental scheme for the realization of an all-optical heat engine in the underdamped regime. We have performed numerical simulations of the stochastic engine using realistic parameters. Further, we have developed an efficient optimization procedure that allows us to determine the optimal driving protocols to any desired accuracy in a systematic manner. These optimal protocols increase the power output and the efficiency of the engine by introducing rapid changes in the trapping frequency. Being able to realize this kind of fast control experimentally is a distinct advantage of the all-optical nature of the heat engine. As we have shown, levitated cavity optomechanics is a powerful novel tool for the study of far-from-equilibrium thermodynamics in the underdamped regime. An extension of our analysis to the full quantum mechanical case is possible, accompanying strong experimental efforts to push levitated systems to operate in the quantum regime [20].

This work was partially supported by the EU Collaborative Project TherMiQ (Grant Agreement No. 618074) and the COST Action Grant No. MP1209.

[1] G. Cerefolini, *Nanoscale Devices*, (Springer, Berlin, 2009).
[2] K. Sekimoto, *Stochastic Energetics*, (Springer, Berlin, 2010).
[3] U. Seifert, Rep. Prog. Phys. **75**, 126001 (2012).
[4] C. Jarzynski, Annu. Rev. Condens. Matter Phys. **2**, 329 (2011).
[5] S. Ciliberto, R. Gomez-Solano, and A. Petrosyan, Annu. Rev. Condens. Matter Phys. **4**, 235 (2013).
[6] A. D. O'Connell, M. Hofheinz, M. Ansmann, R. C. Bialczak, M. Lenander, E. Lucero, M. Neeley, D. Sank, H. Wang, M. Weides, J. Wenner, J. M. Martinis, and A. N. Cleland, Nature (London) **464**, 697 (2010).
[7] J. D. Teufel, T. Donner, D. Li, J. W. Harlow, M. S. Allman, K. Cicak, A. J. Sirois, J. D. Whittaker, K. W. Lehnert, and R. W. Simmonds, Nature (London) **475**, 359 (2011).
[8] J. Chan, T. P. M. Alegre, A. H. Safavi-Naeini, J. T. Hill, A. Krause, S. Groblacher, M. Aspelmeyer, and O. Painter, Nature (London) **478**, 89 (2011).
[9] T. A. Palomaki, J. D. Teufel, R. W. Simmonds, and K. W. Lehnert, Science **342**, 710 (2013).
[10] J. Millen, T. Deesuwan, P. Barker, and J. Anders, Nat. Nanotechnol. **9**, 425 (2014).
[11] V. Blickle and C. Bechinger, Nat. Phys. **8**, 143 (2011).
[12] O. Abah, J. Roßnagel, G. Jacob, S. Deffner, F. Schmidt-Kaler, K. Singer, and E. Lutz, Phys. Rev. Lett. **109**, 203006 (2012).
[13] J. Roßnagel, O. Abah, F. Schmidt-Kaler, K. Singer, and E. Lutz, Phys. Rev. Lett. **112**, 030602 (2014).
[14] K. Zhang, F. Bariani, and P. Meystre, Phys. Rev. Lett. **112**, 150602 (2014).
[15] F. Marquardt, J. P. Chen, A. A. Clerk, and S. M. Girvin, Phys. Rev. Lett. **99**, 093902 (2007).
[16] C. Genes, D. Vitali, P. Tombesi, S. Gigan, and M. Aspelmeyer, Phys. Rev. A **77**, 033804 (2008).
[17] I. Wilson-Rae, N. Nooshi, J. Dobrindt, T. J. Kippenberg, and W. Zwerger, New J. Phys. **10**, 095007 (2008).
[18] D. E. Chang, C. A. Regal, S. B. Papp, D. J. Wilson, J. Ye, O. Painter, H. J. Kimble, and P. Zoller, Proc. Natl. Acad. Sci. U.S.A. **107**, 1005 (2010).
[19] P. F. Barker and M. N. Shneider, Phys. Rev. A **81**, 023826 (2010).
[20] O. Romero-Isart, M. L. Juan, R. Quidant, and J. I. Cirac, New J. Phys. **12**, 033015 (2010).
[21] D. E. Kirk, *Optimal Control Theory*, (Dover, Mineola, 1998).
[22] T. Schmiedl and U. Seifert, Phys. Rev. Lett. **98**, 108301 (2007).
[23] E. Aurell, C. Mejia-Monasterio, and P. Muratore-Ginanneschi, Phys. Rev. Lett. **106**, 250601 (2011).
[24] T. Schmiedl and U. Seifert, Europhys. Lett. **81**, 20003 (2008).
[25] A. Gomez-Marin, T. Schmiedl, and U. Seifert, J. Chem. Phys. **129**, 024114 (2008).
[26] N. Kiesel, F. Blaser, U. Delic, D. Grass, R. Kaltenbaek, and M. Aspelmeyer, Proc. Natl. Acad. Sci. U.S.A. **110**, 14180 (2013).
[27] V. B. Braginsky, A. B. Manukin, and M. Yu. Tikhonov, Sov. Phys. JETP **31**, 829 (1970).
[28] M. Aspelmeyer, T. J. Kippenberg, and F. Marquardt, Rev. Mod. Phys. **86**, 1391 (2014).
[29] We assume that any noise introduced by these light fields is negligible compared to the thermal noise [30].
[30] P. Rabl, C. Genes, K. Hammerer, and M. Aspelmeyer, Phys. Rev. A **80**, 063819 (2009).
[31] Note that the optomechanical cooling may result in a deviation from the thermal equilibrium state for the mechanical oscillator. This effect, however, is negligible for the parameter regime we discuss here.
[32] See Supplemental Material at http://link.aps.org/supplemental/10.1103/PhysRevLett.114.183602 for a summary of the relevant background on cavity-optomechanics and for details on experimental aspects and the numerical optimization, which includes Refs. [33–36].
[33] S. G. Johnson, The NLOPT Nonlinear Optimization Package, 2014, http://ab-initio.mit.edu/nlopt.
[34] W. H. Press, S. A. Teukolsky, W. T. Vetterling, and B. P. Flannery, *Numerical Recipes in Fortran 77: The Art of Scientific Computing*, (Cambridge University Press, New York, 2001).
[35] P. Kaelo and M. M. Ali, J. Optim. Theory Appl. **130**, 253 (2006).
[36] M. D. Powell, Acta Numer. **7**, 287 (1998).
[37] We have optimized with up to 20 parameters ($n = 5$) and did not observe any substantial improvement compared to $n = 3$ (12 parameters).
[38] F. L. Curzon and B. Ahlborn, Am. J. Phys. **43**, 22 (1975).